System-level immune monitoring reveals new pathophysiological features in hepatitis-associated aplastic anemia

Cecile Braudeau, Laurence Delbos, Marie-Laure Couec, Gwenvael Danic, Justine Chevreuil, Camille Lecuroux, Audrey Grain, Marion Eveillard, Fanny Rialland, Flore Sicre de Fontbrune, et al.

RESEARCH LETTER

blood advances

TO THE EDITOR:

System-level immune monitoring reveals new pathophysiological features in hepatitis-associated aplastic anemia

Cecile Braudeau,[1,2] Laurence Delbos,[2] Marie-Laure Couec,[3] Gwenvael Danic,[2] Justine Chevreuil,[1] Camille Lecuroux,[1,2] Audrey Grain,[3] Marion Eveillard,[4] Fanny Rialland,[3] Flore Sicre de Fontbrune,[5] Gaelle Beriou,[2] Nicolas Degauque,[2] David Michonneau,[5,6] Regis Josien,[1,2] Régis Peffault de Latour,[5-7] Caroline Thomas,[3] and Jerome C. Martin[1,2]

[1]Laboratoire d'Immunologie, CHU Nantes, Centre d'Immunomonitorage Nantes Atlantique, [2]CHU Nantes, INSERM, Center for Research in Transplantation and Translational Immunology, UMR 1064, Institut de transplantation urologie-néphrologie, [3]CHU Nantes, Service d'Oncologie-Hématologie et Immunologie Pédiatrique, and [4]Laboratoire d'Hematologie, CHU Nantes, Nantes Université, Nantes, France; [5]Hematology Transplantation, Saint-Louis Hospital, Paris, France; [6]Université Paris Cité, INSERM U976, Paris, France; and [7]Reference Center for Aplastic Anemia and Paroxysmal Nocturnal Hemoglobinuria, Saint-Louis Hospital, Paris, France

Hepatitis-associated aplastic anemia (HAA) is a variant of immune AA in which bone marrow failure (BMF) occurs within 6 months of an episode of acute hepatitis.[1-5] Spectratyping studies revealed a skewed T-cell repertoire within liver-infiltrating T cells, which was mirrored in the blood at time of BMF, and reversed upon successful immunosuppression.[5] These data suggest that relevant immune perturbations in HAA can be captured in the blood and monitored during disease progression from hepatitis to BMF.

High-dimensional flow cytometric analysis was applied to characterize blood immune cell profiles of 3 patients with HAA and in 1 pediatric and 1 adult healthy control (HC) (supplemental Tables 1-3). Immune remodeling during HAA progression was monitored in case 1 (HAA-1) through 4 iterative analyses spanning days 9 to 78 after initial symptom onset (supplemental Figure 1A). HAA-2 and HAA-4 matched the kinetics of the latest sample of HAA-1 (>day 70 after initial symptom onset). Opt-SNE projections of concatenated data for $CD45^{+}$ leucocytes from all samples, followed by FlowSOM clustering, revealed 9 immune metaclusters (supplemental Figure 1B-C; supplemental Table 4). Granulocytes and monocytes were severely reduced in HAA and kinetic analyses in HAA-1 verified their progressive decrease (supplemental Figure 1D-E; supplemental Table 2). Absolute lymphocyte counts were reduced (supplemental Table 3) but, despite alterations at earlier time points, proportions of the main populations ultimately converged to reference values (supplemental Figure 1F-H).[6] An overrepresentation of B cells was further investigated using manual gating strategies to reveal increased immature $CD38^{++}$ $CD24^{++}$ transitional B cells at day 9 and day 16. At late time points, B-cell subsets aligned with reference values (supplemental Figure 2A-F).[7] Written informed consent for all individuals in this study was provided in compliance with an institutional review board protocol and the declaration of Helsinki and good clinical practice principles.

Altered T-cell proportions included an inverted CD4:CD8 ratio, a feature known in HAA,[4] and a previously unappreciated expansion of γδ T cells, which represented up to 26% of T cells at day 16 (Figure 1A). Expansions of transitional B cells and γδ T cells existed before steroid introduction at day 11, thus, ruling out medication as the main driver of lymphocyte qualitative remodeling. To characterize further the significance of T-cell alterations in HAA, an exploratory analysis was conducted by generating new opt-SNE projections specifically on T cells, with the aim of obtaining a more granular definition of the various T-cell phenotypes encountered in the data set. Key regions of the opt-SNE map were found in HAA and corresponded to CD8 T cells and γδ T cells, part of which expressed the activation marker HLA-DR (supplemental Figure 3A-B). FlowSOM clustering revealed 21 T-cell

Submitted 2 June 2022; accepted 20 May 2023; prepublished online on *Blood Advances* First Edition 2 June 2023; final version published online 28 July 2023. https://doi.org/10.1182/bloodadvances.2022008224.

FCS files have been deposited in FlowRepository under accession number FR-FCM-Z5DK (https://flowrepository.org/id/RvFr1irFNLjdalDG0lsm2V882JC3HkUOcoraeaOy3eDkRZ2wyJdQyU7FPNEqXeLK). Additional data are available on request from the corresponding author, Jerome C. Martin (jerome.martin@univ-nantes.fr).

The full-text version of this article contains a data supplement.

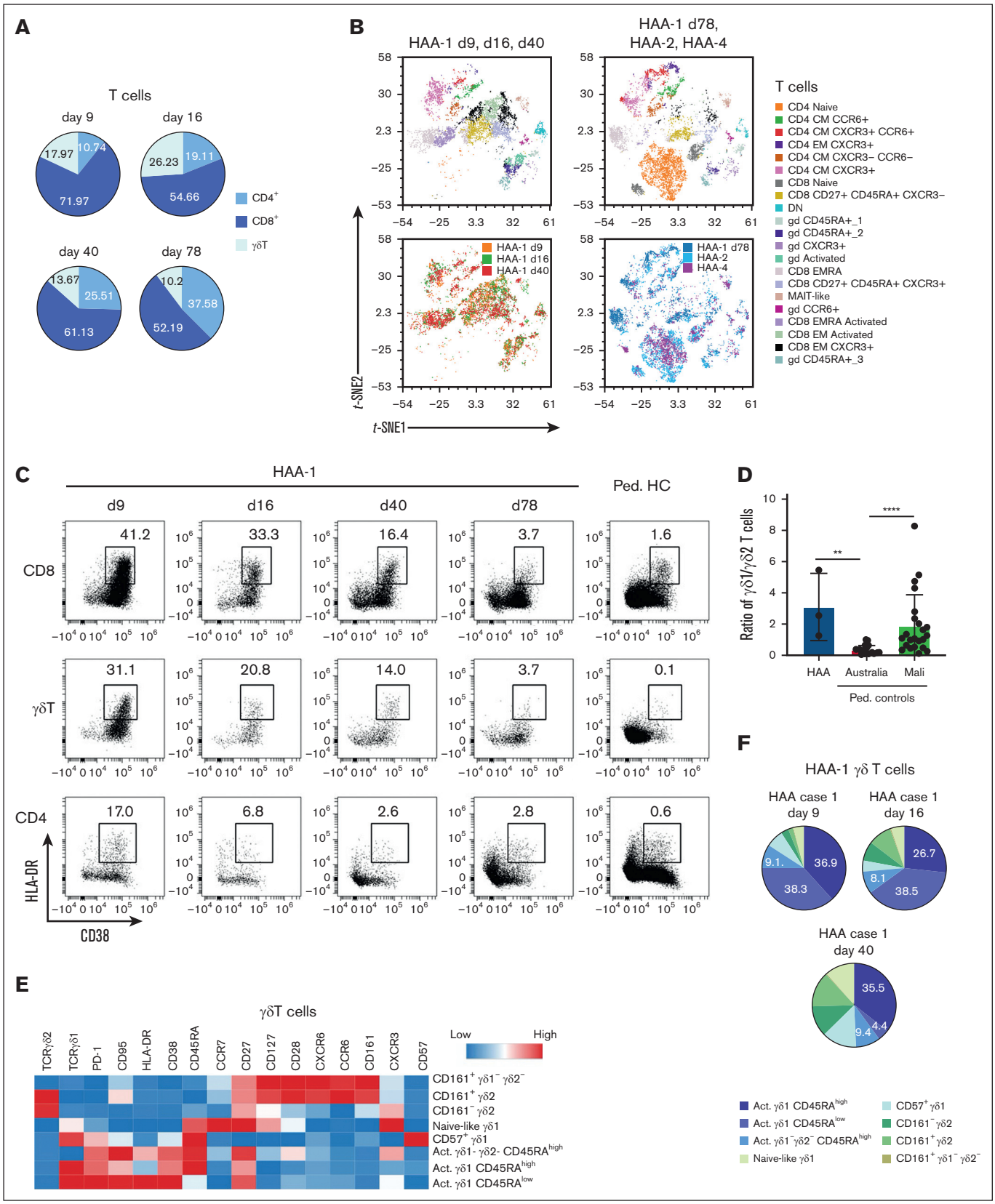

Figure 1. A Vδ1+ γδ T-cell acute response with long-term alterations in HAA. (A) Pie charts representing the percentage of indicated T-cell subsets within total blood T cells at 4 time points after disease onset for HAA case 1. (B) Opt-SNE projections of concatenated cytometry data for T cells from patient HAA-1 samples at early time points day 9, day 16, and day 40 (left), and HAA-1 day 78, HAA-2 and HAA-4 (right). Cells are grouped and annotated into color-coded metaclusters after FlowSOM clustering (top) or

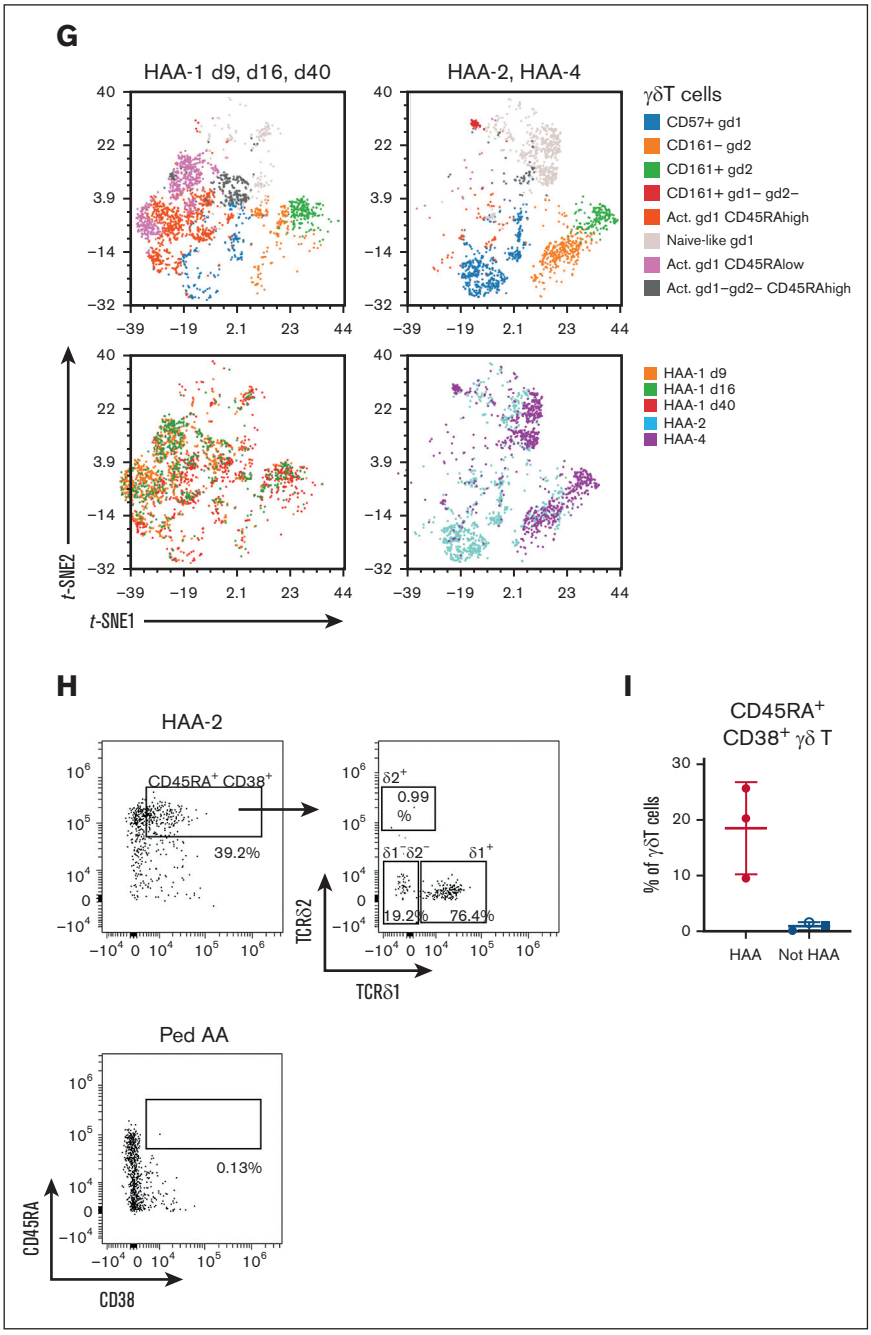

Figure 1 (continued) by sample origin (bottom). (C) Flow cytometry plots quantifying manually gated HLA-DR$^+$ CD38$^+$ activated cells within total CD8 T cells, γδ T cells, and CD4 T cells from HAA-1 and pediatric (ped.) HC. Numbers correspond to the percentage of activated cells within the corresponding T-cell subset. (D) Dot plots comparing the ratio of γδ1:γδ2 T cells between patients with HAA (n = 3 patients, >70 days after initial symptom onset) and pediatric HCs from Australia and Mali.[8] Error bars indicate mean ± standard deviation; data analyzed by Kruskal-Wallis analysis of variance with Dunn posttest comparisons. $^{**}P = .0039$ and $^{****}P < .0001$. (E) Heatmap showing the relative expression of relevant membrane markers used to annotate FlowSOM metaclusters (color scale: row-adjusted z-score expression for each individual marker). (F) Pie charts representing the percentage of γδ T-cell metaclusters within total γδ T cells at 3 time points after disease onset for HAA-1. (G) Opt-SNE projections of concatenated cytometry data for γδ T cells from HAA-1 samples at early time points day 9, day 16, and day 40 (left), and HAA-2 and HAA-4 (right). Cells are grouped and annotated into color-coded metaclusters after FlowSOM clustering (top) or by sample origin (bottom). (H) Left: representative flow cytometry plots of manually gated CD45RA$^+$ CD38$^+$ γδ T cells within total CD57$^-$ γδ T cells for HAA-2 and control pediatric AA. Numbers represent the percentage of indicated CD45RA$^+$ CD38$^+$ γδ T cells. Right: representative flow cytometry plots of manually gated γδ1$^+$, γδ2$^+$, and γδ1$^-$γδ2$^-$ cells within CD45RA$^+$ CD38$^+$ γδ T cells in HAA-2. Numbers represent the percentage of indicated subset in total CD45RA$^+$ CD38$^+$ γδ T cells. (I) Dot plot comparing the percentage of CD57$^-$ CCR7$^-$ CD45RA$^+$ CD38$^+$ γδ T cells between patients with HAA at late disease stage (n = 3) and controls (nonhepatitis pediatric AA: black dot; pediatric HC: black square; adult HC: white dot).

metaclusters (supplemental Figure 3C; supplemental Table 4). Although samples from the late HAA-1 time point and to the 2 other patients with HAA displayed similar cell distributions, this was not the case for cells from samples collected from patient HAA-1 at early time points (Figure 1B). Populations of HLA-DR$^+$ CD38$^+$ activated CD8 and γδ T cells were indeed largely enriched in patient HAA-1 between day 9 and day 40 (supplemental Figure 3D-E). However, the inability to include samples from early time points of patients HAA-2 and HAA-4 could introduce a limitation by raising the possibility that skewed T-cell phenotypes could be obtained by the analysis of multiple samples from patient HAA-1 only. A manual gating strategy to analyze HLA-DR and CD38 validated the increased proportions of activated CD8 and γδ T cells in patient HAA-1 samples from early time points (Figure 1C). Activated CD8 T cells in patient HAA-1 were identified with effector memory (CD45RA$^-$ CCR7$^-$) and effector memory CD45RA re-expressing (CD45RA$^+$ CCR7$^-$) phenotypes (supplemental Figure 3D). Activated effector memory CD8 T cells accounted for 20% of T cells at day 9 and progressively decreased to control levels at day 78. Activated effector memory CD45RA re-expressing CD8 T cells, in turn, increased their frequencies up to 10% of T cells at day 40, hence, suggesting that the latter could represent a terminally differentiated state of the former (supplemental Figure 3F). Activated γδ T cells followed similar kinetics as CD8 T cells (Figure 1C; supplemental Figure 3F). Activated CD8 and γδ T cells were detectable at day 40, when liver function was restored but not AA, and the ratio of activated CD8/activated γδ T cells remained constant at all 3 time points (Figure 1C; supplemental Figure 3G). Interestingly, although proportions of conventional T-cell metaclusters were similar between controls and late-stage HAA (>day-70 after initial symptom onset), CD45RA$^+$ γδ T cells remained consistently increased in HAA (supplemental Figure 3H-I).

The Vδ2$^+$/Vγ9$^+$ subset dominates the γδ T-cell compartment in human peripheral blood, whereas the liver is enriched for Vδ1$^+$ γδ T cells.[9-11] To explore whether activated γδ T cells could be of liver origin, a new flow cytometric analysis was applied to frozen whole-blood aliquots.[12] Remarkably, patients with HAA displayed significantly higher Vδ1$^+$/Vδ2$^+$ ratios in comparison to pediatric HCs (Figure 1D).[8] No difference, in turn, existed between patients with HAA and a pediatric cohort who had experienced oligoclonal selection, differentiation, and expansion of Vδ1$^+$ T cells in response to repeated *Plasmodium falciparum* infections. To more precisely define γδ T-cell phenotypes present in the data set, opt-SNE projections followed by FlowSom clustering were generated, which identified 8 γδ T-cell metaclusters, including Vδ2$^+$, Vδ1$^+$, and Vδ2$^-$/Vδ1$^-$ populations (supplemental Figure 3J). The phenotypic analysis revealed that activation markers HLA-DR and CD38 were restricted to Vδ1$^+$ and Vδ2$^-$/Vδ1$^-$ subsets (Figure 1E). Kinetic analysis in patient HAA-1 suggested that CD45RA^{high} CD38$^+$ HLA-DR$^{low/-}$ CCR7$^-$ Vδ1$^+$ T cells dominated the Vδ1$^+$ T-cell compartment at day 40 (Figure 1F). Of note, these populations were virtually absent in a patient with immune AA not associated with hepatitis (supplemental Figure 3K). As for the T-cell analysis discussed earlier, a risk existed that γδ T-cell phenotypes were skewed by the inclusion of multiple samples from patient HAA-1 at early time points (Figure 1G). To test the hypothesis that a persistent remodeling of the γδ T-cell compartment characterized by increased proportions of CD45RA^{high} CD38$^+$ CD57$^-$ CCR7$^-$ Vδ1$^+$ γδ T cells could be generalized to the 3 patients with HAA included in the study at late time points after initial symptom onset, we used a manual gating strategy to directly compare this population between controls and patients with HAA (Figure 1H; supplemental Figure 4B). This analysis validated the consistent increased proportions of CD45RA^{high} CD38$^+$ CD57$^-$ CCR7$^-$ Vδ1$^+$ γδ T cells in the blood of HAA patients as compared with controls (Figure 1I; supplemental Figure 4B), though this must be interpreted in a context of severe T-cell lymphopenia in HAA patients. Another limitation of this analysis was the impossibility to directly compare absolute counts of the γδ T-cell subsets between HAA and HCs. Previous work from others indicated that, unlike liver-resident effector CD45RA$^-$ Vδ1$^+$ T cells, clonally expanded effector CD45RA$^+$ Vδ1$^+$ T cells recirculate between blood and liver.[11] Altogether, these data thus suggest a liver origin for the CD45RA^{high} CCR7$^-$ Vδ1$^+$ T cells enriched in blood of patients with HAA.

Plasma cytokines were analyzed in 4 patients with HAA and 7 HCs (supplemental Table 5). Hypothesizing that pathways active in HAA should involve coordinated secretions of multiple ligands, a correlation matrix was realized to identify cytokine modules (Figure 2A). Module a comprised interferon γ (IFN-γ), interleukin 18 (an IFN-γ inducer in lymphocytes),[13] and CXCL10 (an IFN-γ–inducible chemokine in mononuclear phagocytes),[14,15] hence reflecting a type 1 immune response. Module a expression was low at late-stage HAA but high during early stages in patient HAA-1 (Figure 2B-C), with kinetics paralleling those of activated CD8 and Vδ1$^+$ γδ T cells. Interleukin-12p70 also correlated with IFN-γ levels (Figure 2A; supplemental Figure 4H). Intracellular cytokine analysis revealed that >90% of CD4$^-$ T cells were positive for IFN-γ at day 9 (Figure 2D), indicating that CD8 T and γδ T cells both contributed to systemic IFN-γ levels. Interestingly, activated CD8 T and γδ T cells expressed CXCR3, the receptor for CXCL10 (supplemental Figure 4C). In contrast, no major IFN-γ expression was detected in CD4$^+$ T cells and innate lymphocytes (Figure 2D; supplemental Figure 4D-E). CD8 and γδ T cells maintained a skewed type 1 immune response at late disease stages (supplemental Figure 4D).

Module b comprised chemokines produced by inflammatory macrophages (CCL3, CCL4, and CXCL8) (Figure 2A),[16] which remained high in late-stage disease (Figure 2E), suggesting sustained macrophage activation in HAA. Accordingly, BM smears from patient HAA-1 contained macrophages with hyperbasophilic cytosols enriched with vacuoles (Figure 2F). Hemophagocytic activity was also observed, indicating that macrophage-mediated progenitor destruction could extend beyond the previously described TNF-dependent mechanisms.[17] Compared with controls and reference values,[18] a low classical-to-nonclassical monocyte ratio existed in the blood as early as day 9 after initial symptom onset, and was verified for all 3 patients (Figure 2G; supplemental Figure 1E). This could be explained by several nonmutually exclusive mechanisms, including faster maturation and/or death rates, increased peripheral tissue infiltration, or increased retention of classical monocytes in the BM. In support of the latter, recent mouse data suggest that IFN-γ–dependent BM failure during severe immune AA relied on the expression of CCR5 to maintain macrophages in the BM.[19] Remarkably, CCL5 levels, the ligand for CCR5, were reduced in HAA (Figure 2H; supplemental Figure 4F). Activated BM macrophages trigger CXCL12 expression in nestin$^+$ CXCL12-abundant reticular cells for the retention of hematopoietic stem cell progenitors.[20] Supporting possible relationships between myeloid and stromal activation in the BM of patients with HAA,

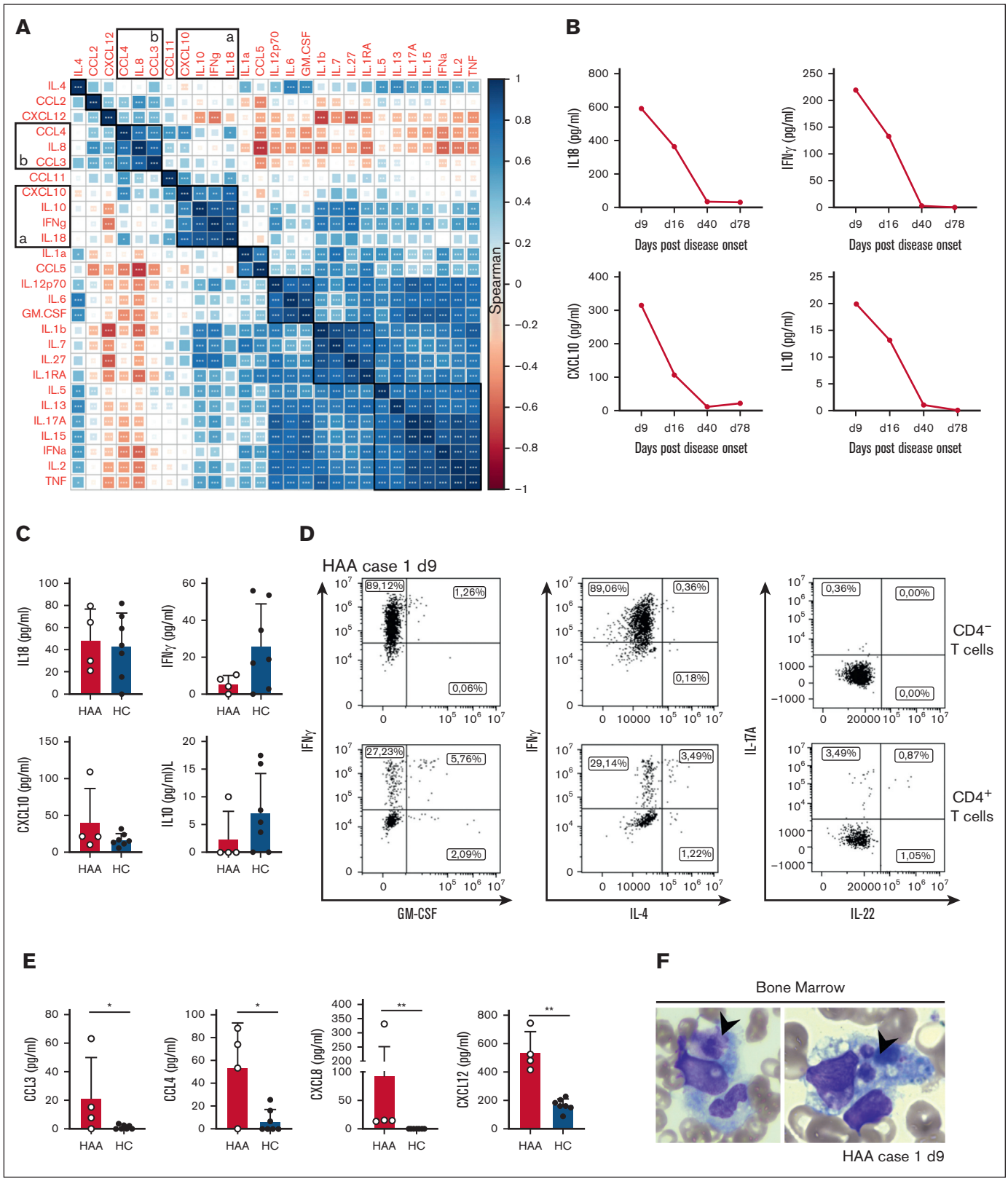

Figure 2. A type-1 immune environment contributed by γδ T and CD8 T cells in HAA. (A) Spearman correlation and hierarchical clustering of indicated cytokines measured in the serum of HAA cases (n = 4 patients; 4 time points were collected for HAA-1; 7 samples in total) and HC (pediatric, n = 1; adult, n = 6). (B) Dot plots representing the level of indicated cytokine at 4 time points after disease onset for HAA-1. (C) Comparison of cytokine levels between HAA (n = 4 patients, >70 days after initial symptom onset) and HC. Error bars indicate mean ± standard deviation. (D) Peripheral blood mononuclear cells were stimulated for 3 hours with PMA and ionomycin and analyzed for intracellular

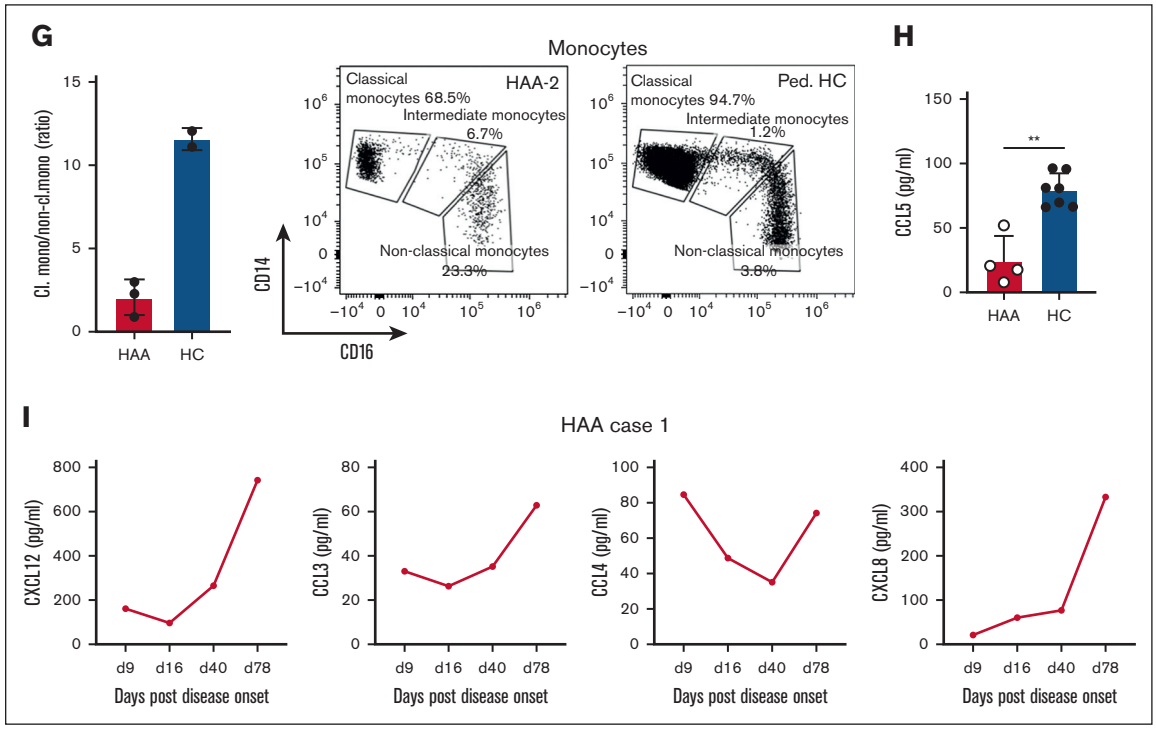

Figure 2 (continued) cytokine production. Flow cytometry plots show the expression of indicated cytokines in $CD4^+$ and $CD4^-$ T cells obtained from HAA-1 at day 9 after initial symptom onset. (E) Comparison of cytokine levels between HAA (n = 4 patients, >70 days after symptom onset) and HC. Error bars indicate mean ± standard deviation; data analyzed by 2-sided Mann-Whitney *U* test. $*P < .05$ and $**P < .01$. (F) HAA-1 BM smear was obtained at day 9 and colored with May-Grünwald-Giemsa (MGG) stain. Representative pictures of activated macrophages. Arrows indicate hemophagocytosis. (G) Left: ratio of classical-to-nonclassical monocytes defined after FlowSOM metaclustering in patients with HAA at late-stage disease (n = 3) and HCs. Right: representative manual gating of blood monocyte subsets in patients with HAA and HCs. (H) Comparison of CCL5 levels between patients with HAA (n = 4 patients at >70 days after symptom onset) and HCs. Error bars indicate mean ± standard deviation; data analyzed by 2-sided Mann-Whitney *U* test. $**P < .01$. (I) Dot plots representing the level of indicated cytokine at 4 time points after disease onset for HAA-1.

CXCL12 significantly correlated with the myeloid chemokines (Figure 2A). Accordingly, higher CXCL12 levels were detected in patients with HAA, which progressively increased with disease evolution in patient HAA-1 (Figure 2E,I).

In conclusion, this study provides new pathophysiological insights that more specifically define HAA within the whole spectrum of immune AA, and offers a rational basis for new research directions aimed at exploring disease mechanisms, as well as new biomarker and therapeutic opportunities (supplemental Discussion). The main limitations of this work are related to the small cohort size, especially for the early HAA time points showing the acute Vδ1 γδ T-cell activation, which could only be analyzed in a single patient.

Acknowledgments: The authors thank Julie Déchanet-Merville (ImmunoConcEpT, Centre National de la Recherche Scientifique, Unité Mixte de Recherche 5164, University of Bordeaux) and Ephraim Kenigbserg (Genentech) for critical reading and scientific inputs to the manuscript.

J.C.M. is supported by NExT "Junior Talent", ANR JCJC (ANR-20-CE17-0009) and ARC Programmes labellisés (PGA).

Contribution: J.C.M. conceptualized the study, performed formal analysis, developed the methodology, supervised the study, and wrote the original draft of the manuscript; C.B., L.D., C.L., and N.D. performed data curation; C.B., L.D., M.L.-C., G.D., M.E., J.C., C.L., A.G., F.R., G.B., and C.T. conducted the investigation; C.B., L.D., N.D., D.M., R.J., R.P.d.L., C.T., and J.C.M. developed the methodology; N.D. and J.C.M. carried out the data visualization; and F.S.d.F., D.M., R.J., C.T., and J.C.M. wrote, reviewed, and edited the final manuscript.

Conflict-of-interest disclosure: The authors declare no competing financial interests.

ORCID profiles: L.D., 0000-0002-4320-0681; A.G., 0000-0003-1547-8229; M.E., 0000-0001-7206-5135; F.R., 0000-0002-3136-6270; F.S.d.F., 0000-0003-2000-1556; N.D., 0000-0003-2990-3513; D.M., 0000-0003-4553-3065; J.C.M., 0000-0003-0068-8776.

Correspondence: Jerome C. Martin, Centre de Recherche Translationnelle en Transplantation et Immunologie, Nantes Université, 30, Blvd Jean Monnet, F-44000 Nantes, France; email: jerome.martin@univ-nantes.fr.

References

1. Young NS. Aplastic anemia. *N Engl J Med*. 2018;379(17):1643-1656.
2. Gonzalez-Casas R, Garcia-Buey L, Jones EA, Gisbert JP, Moreno-Otero R. Systematic review: hepatitis-associated aplastic anaemia–a

syndrome associated with abnormal immunological function. *Aliment Pharmacol Ther*. 2009;30(5):436-443.

3. Marsh JCW, Ball SE, Darbyshire P, et al. Guidelines for the diagnosis and management of acquired aplastic anaemia. *Br J Haematol*. 2003; 123(5):782-801.
4. Brown KE, Tisdale J, Barrett AJ, Dunbar CE, Young NS. Hepatitis-associated aplastic anemia. *N Engl J Med*. 1997;336(15):1059-1064.
5. Lu J, Basu A, Melenhorst JJ, Young NS, Brown KE. Analysis of T-cell repertoire in hepatitis-associated aplastic anemia. *Blood*. 2004; 103(12):4588-4593.
6. Ding Y, Zhou L, Xia Y, et al. Reference values for peripheral blood lymphocyte subsets of healthy children in China. *J Allergy Clin Immunol*. 2018;142(3):970-973.e8.
7. Morbach H, Eichhorn EM, Liese JG, Girschick HJ. Reference values for B cell subpopulations from infancy to adulthood. *Clin Exp Immunol*. 2010;162(2):271-279.
8. von Borstel A, Chevour P, Arsovski D, et al. Repeated Plasmodium falciparum infection in humans drives the clonal expansion of an adaptive γδ T cell repertoire. *Sci Transl Med*. 2021;13(622): eabe7430.
9. Davey MS, Willcox CR, Baker AT, Hunter S, Willcox BE. Recasting human Vδ1 lymphocytes in an adaptive role. *Trends Immunol*. 2018; 39(6):446-459.
10. Hayday AC. γδ T cell update: adaptate orchestrators of immune surveillance. *J Immunol*. 2019;203(2):311-320.
11. Hunter S, Willcox CR, Davey MS, et al. Human liver infiltrating γδ T cells are composed of clonally expanded circulating and tissue-resident populations. *J Hepatol*. 2018;69(3):654-665.
12. Braudeau C, Salabert-Le Guen N, Chevreuil J, Rimbert M, Martin JC, Josien R. An easy and reliable whole blood freezing method for flow cytometry immuno-phenotyping and functional analyses. *Cytometry B Clin Cytom*. 2021;100(6):652-665.
13. Kaplanski G. Interleukin-18: biological properties and role in disease pathogenesis. *Immunol Rev*. 2018;281(1):138-153.
14. Dufour JH, Dziejman M, Liu MT, Leung JH, Lane TE, Luster AD. IFN-gamma-inducible protein 10 (IP-10; CXCL10)-deficient mice reveal a role for IP-10 in effector T cell generation and trafficking. *J Immunol*. 2002;168(7):3195-3204.
15. Luster AD, Ravetch JV. Biochemical characterization of a gamma interferon-inducible cytokine (IP-10). *J Exp Med*. 1987;166(4):1084-1097.
16. Mantovani A, Sica A, Sozzani S, Allavena P, Vecchi A, Locati M. The chemokine system in diverse forms of macrophage activation and polarization. *Trends Immunol*. 2004;25(12):677-686.
17. Sun W, Wu Z, Lin Z, et al. Macrophage TNF-α licenses donor T cells in murine bone marrow failure and can be implicated in human aplastic anemia. *Blood*. 2018;132(26):2730-2743.
18. Kapellos TS, Bonaguro L, Gemünd I, et al. Human monocyte subsets and phenotypes in major chronic inflammatory diseases. *Front Immunol*. 2019;10:2035.
19. Seyfried AN, McCabe A, Smith JNP, Calvi LM, MacNamara KC. CCR5 maintains macrophages in the bone marrow and drives hematopoietic failure in a mouse model of severe aplastic anemia. *Leukemia*. 2021; 35(11):3139-3151.
20. Chow A, Lucas D, Hidalgo A, et al. Bone marrow CD169+ macrophages promote the retention of hematopoietic stem and progenitor cells in the mesenchymal stem cell niche. *J Exp Med*. 2011;208(2):261-271.